Antimony and Bismuth Oxide Clusters: Growth and Decomposition of New Magic Number Clusters

M. R. France, J. W. Buchanan, J. C. Robinson, S. H. Pullins, J. L. Tucker, R. B. King, and M. A. Duncan*

Department of Chemistry, University of Georgia, Athens, Georgia 30602

Received: May 20, 1997[⊗]

A series of new "magic number" metal oxide clusters are described for the group V metals antimony and bismuth. Specific nonstatistical stoichiometries of M_xO_y cation and anion clusters are formed preferentially in the gas phase when oxidized metal is vaporized or when metal is vaporized and combined with gas phase oxygen (e.g., $Bi_7O_{10}^+$, $Bi_9O_{14}^+$). Essentially the same stoichiometries are seen for antimony and bismuth analogues. The species produced in cluster growth are also produced preferentially by photodissociation of larger clusters. Localized covalent bonding schemes are suggested for these clusters, and polyhedral cage structures are proposed. The stoichiometries observed require a 3+ metal oxidation state in the small clusters, which shifts over to one or more 5+ metal atoms in larger clusters.

Introduction

Gas phase clusters with closed shell electronic configurations and/or symmetric geometries may lead to "magic numbers", i.e., preferred sizes or stoichiometries, when the distribution produced is observed with mass spectrometry. Dramatic magic numbers have been observed previously for alkali metal clusters,[1] carbon clusters,[2] main group alloy clusters,[3] and metal carbide ("met-cars") clusters,[4−9] revealing fascinating new concepts in chemical bonding and molecular structure. As shown with C_{60} and the fullerenes, stable gas phase clusters may be produced in macroscopic quantities in the condensed phase, leading to new cluster-based materials, and so there is much interest in identifying other cluster systems with similar potential. We report here the observation of a new class of magic number metal cluster *oxides* observed for the main group metals antimony and bismuth. Remarkable preferences are observed for metal oxides with specific stoichiometries explained by straightforward bonding patterns. We investigate bonding patterns and structures for these clusters through mass spectrometry measurements of their growth and photodissociation measurements of their decomposition.

Pure metal clusters of antimony and bismuth have been investigated previously with inert gas condensation sources,[10,11] pulsed nozzle laser vaporization sources,[12] and laser ablation of metal without collisional gases.[13] Magic number patterns generated by these various sources are consistent, and they have been studied for neutral clusters as well as ions of both charge states. Prominent species are different for different charge states, indicating that specific electronic effects (i.e., electron counting) are important in cluster stability.[12] Mass-selected photodissociation studies of cation clusters demonstrate that prominent photofragments correspond to the same species produced preferentially in the cation growth distribution, establishing in independent experiments that the specific species M_3^+, M_5^+, etc. have enhanced stability relative to other clusters.[12] The small negative ion clusters have been studied with photoelectron spectroscopy.[14,15] Consistent with accepted inorganic chemistry concepts,[16] the bonding in these metals is believed to involve primarily the valence p electrons, while the valence s electrons have lower energies and are believed to constitute an "inert pair". The cluster bonding schemes that have been suggested, therefore, lead to stable species having an even number of valence p electrons.

Alloy clusters of the main group elements,[3,17−20] especially including antimony and bismuth,[3] have also been the subject of several investigations. Consistent experiments from different laboratories show that specific nonstatistical stoichiometries are produced in alloy clusters containing antimony and bismuth mixed with the group IV elements tin or lead.[3,18,19] These alloy stoichiometries are understandable by analogy to the well-known Zintl ion clusters,[16,21] which have been studied for many years in condensed phase inorganic chemistry. In the Zintl ion species, and their gas phase metal alloy counterparts, the unique stoichiometries observed are derived primarily from electronic effects in cluster bonding, which can be explained and predicted by Wade's rules of electron counting.[21] These species are electron deficient, and the clusters take on polyhedral structures, making it possible to share electron density in the interior volume of the cluster. Closed shell clusters result for species with n metal atoms and $2n + 2$, $2n + 4$, and $2n + 6$ valence p electrons, corresponding to *closo*, *nido*, and *arachno* cluster series. For example, the condensed phase Zintl ion Pb_5^{2-} has the gas phase alloy analogue $Pb_2Sb_3^+$, while the Zintl ion Sn_9^{4-} has the gas phase analogue $Sn_4Bi_5^+$. While electron counting considerations have been quite successful for alloys of the main group metals, it is not yet clear what concepts in structure and bonding will apply for main group metal compound clusters (i.e., oxides, carbides, nitrides). Interesting results have been obtained recently for transition metal compound clusters,[5−9,22,23] but there are only a few studies of main group metal compounds.[17]

In the oxide clusters of the group V metals studied here, dramatic magic number patterns are observed with unique oxide stoichiometries at each metal size. We investigate these trends with mass spectra under different conditions and with mass-selected photodissociation measurements. The stoichiometries observed, however, are not related to pure metal or metal alloy clusters studied previously for these metals. Instead, it is possible to use simple covalent bonding schemes to rationalize cluster bonding for neutrals, cations, and anions. This process suggests interesting cluster structures corresponding to the specific oxide stoichiometries.

* Author to whom correspondence should be addressed.
[⊗] Abstract published in *Advance ACS Abstracts,* August 15, 1997.

S1089-5639(97)01668-X CCC: $14.00

Experimental Section

Metal oxide clusters observed are formed by laser vaporization of a metal rod in a pulsed nozzle source, with the expansion gas seeded with oxygen, or by laser desorption of a metal powder with partial surface oxidation through exposure to air. These experiments are done in two different machines. The laser desorption mass spectrometer apparatus used has been described previously.[24] Ions are formed in the single acceleration stage of a time-of-flight spectrometer. Oxidized metal powder is pressed into a pellet and mounted on a probe in the center of the acceleration region flush with the surface of the rear acceleration plate. Desorption is accomplished by focusing a Nd:YAG laser (Continuum Minilite) at 532 nm on the metal pellet surface. Cluster ions are formed by the vaporization process with no collision gas present to enhance growth and are then accelerated into the 1.5-m time-of-flight tube by pulsed acceleration voltages. Delayed pulse acceleration techniques are employed to enhance resolution. An einzel lens and deflection plates are used to focus ions onto the detector. Ions are detected by an electron multiplier tube (Hamamatsu R-595). Signals are collected by a digital oscilloscope (LeCroy 9310A) and recorded on a PC via an IEEE-488 interface.

In the molecular beam machine, clusters are produced by laser vaporization in a pulsed nozzle source. The pulsed nozzle source using a modified Newport Corporation BV-100[25] valve and the molecular beam apparatus used[26] are described in previous reports from our research group. Metal oxide clusters are formed by vaporization of a metal rod with a focused XeCl excimer laser (Lumonics 860) at 308 nm in an expansion of 6% O_2 in helium. The clusters grow in a channel after the point of vaporization. The growth channel consists of a segment 20 mm long with a 2-mm diameter and another segment 10 mm long with a 4-mm diameter. The gas mixture is collimated into a molecular beam as it passes through a skimmer into the mass spectrometer.

Cation clusters formed directly in the laser vaporization cluster source are extracted from the molecular beam by pulsed acceleration voltages. Neutral clusters formed in the cluster source are photoionized by a laser crossing perpendicular to the molecular beam in the mass spectrometer ion source. Photoionization is accomplished with an ArF excimer laser (Lumonics PM-842) at 193 nm. Photoionized clusters are extracted by dc voltages applied to the acceleration plates. A specially designed reflectron time-of-flight mass spectrometer makes it possible to measure the cluster distributions produced from the source or to mass select clusters for photodissociation experiments.[27] Photodissociation occurs at the turning point in the reflectron and is accomplished with a Nd:YAG laser (Spectra Physics GCR-170) at 355 nm. The photodissociation mass spectra are recorded using a computer difference technique. Ions are detected by an electron multiplier tube, and mass spectra are recorded with a digital oscilloscope (LeCroy 9410) interfaced to a PC.

Results and Discussion

Initial studies were conducted on oxidized antimony and bismuth samples in the laser desorption mass spectrometer. In this instrument, there is no collision gas or ionization laser. Ions are formed directly by the vaporization laser in the source of the mass spectrometer and accelerated immediately down the flight tube. Metal cluster formation for pure antimony and bismuth under these conditions has been observed previously by McElvaney and co-workers.[13] The sample was metal powder pressed into a depression in the sample holder, and oxidation occurred unintentionally by exposure to ambient air. After oxide clusters were observed and found to be interesting, additional studies of oxidation conditions were conducted. The mass spectra observed for cation clusters of bismuth are shown in Figure 1. The upper trace shows the lower mass region where intense mass peaks are observed, while the lower trace shows the higher mass region detected with different deflection plate focusing.

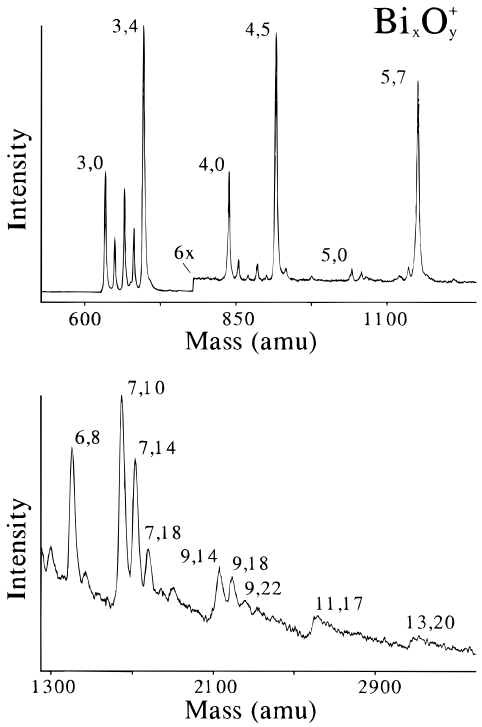

Figure 1. Mass spectrum of bismuth oxide cluster cations produced by laser desorption of a partially oxidized metal powder sample with no collision gas present. The upper trace shows the lower mass region, while the lower trace shows an amplified view of the high-mass region.

These data for bismuth show the production of pure metal clusters and certain metal oxides. The most interesting observation in this data is that the oxide stoichiometries produced are not random or statistical. In the low-mass region, there is one specific oxide stoichiometry at each cluster size (number of metal atoms) which is much more prominent than the others (e.g. $M_3O_4^+$). In some cases, only one oxide stoichiometry is observed ($M_5O_7^+$). Although we do not show the antimony data here, the stoichiometries observed for Sb/O cluster cations produced this same way are the same as those for bismuth. Prominent stoichiometries for both metals are $M_3O_4^+$, $M_4O_5^+$, and $M_5O_7^+$. These prominent metal oxide cations in the small size domain have been reported many years ago under laser desorption mass spectrometer conditions.[28−31] However, no clusters larger than about five metal atoms were observed and no explanations were given for these trends.

The lower trace of Figure 1 shows the mass spectra observed when the instrument is focused in the higher mass range for bismuth clusters. The signal intensity is weak but reproducible for bismuth, which has a single isotope, but it is too weak to be detected for antimony. Antimony has two naturally occurring isotopes (57% ^{121}Sb, 43% ^{123}Sb), and so the reduced sensitivity at large cluster sizes is attributed to the much broader isotope distribution. For the bismuth system, oxidized clusters are detected containing up to 13 metal atoms. Prominent stoichiometries are $M_6O_8^+$, $M_7O_{10}^+$, $M_7O_{14}^+$, $M_7O_{18}^+$, $M_9O_{14}^+$, $M_9O_{18}^+$, and $M_{11}O_{17}^+$. Thus, some cluster sizes exhibit two or three oxides, but the distribution of oxides is still far from random.

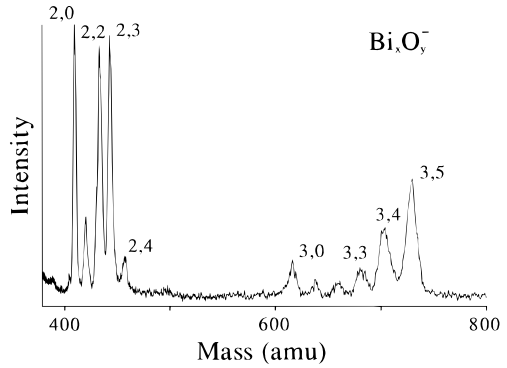

Figure 2. Mass spectrum of bismuth oxide cluster anions produced by laser desorption of a partially oxidized metal powder sample with no collision gas present.

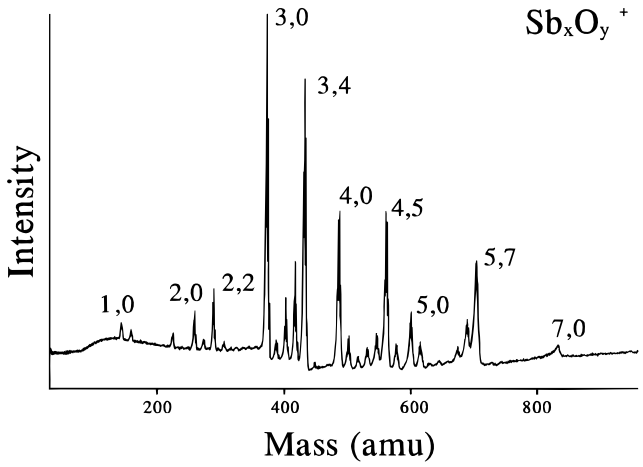

Figure 3. Mass distribution of antimony/oxygen cation clusters produced in the laser vaporization cluster source with helium expansion gas seeded with oxygen.

When specific clusters are produced preferentially, it is possible to invoke either geometric or electronic structure effects to explain the prominent species formed. An important test for these effects is the study of clusters having different charge states. If electronic effects are prominent, clusters having the same approximate number of atoms may exhibit different preferences in formation for different charge states. Figure 2 shows the masses produced in the same kind of laser desorption experiment for the negative ion species. Unfortunately, negative ion species are extremely difficult to produce under these conditions, but two observations are possible. In the positive ions, there is a sharp drop-off after $Bi_2O_2^+$ (i.e. 2/2), but the negative ions show the formation of the larger species 2/3 and a small amount of 2/4. In the M_3 region, the 3/4 cation is extremely abundant, with no evidence for larger oxides at this metal size, while the negative ions have a strong 3/5 preference. These effects are reproducible, and they provide strong evidence for electronic structure effects in the small cluster bonding. We would of course like to measure the same effects for larger negative ions, but we have so far been unable to produce these species.

Having seen these effects in cluster growth in a source with no collision gas present, we were interested in investigating these cluster systems in our normal molecular beam cluster sources. Figure 3 shows an example of antimony/oxygen clusters produced when a metal rod is vaporized with a focused laser in an expansion of helium seeded with oxygen, using a molecular beam cluster source of standard design. The cluster cations produced directly in the source are measured with pulsed extraction from the molecular beam into the time-of-flight mass spectrometer system. The mass distribution is nearly the same as that produced in the laser desorption mass spectrometer experiment, with pure metal clusters and specific metal oxide clusters observed. The bismuth distribution under these same conditions is essentially the same as that for antimony. Again, the 3/4, 4/5, and 5/7 stoichiometries are observed as abundant oxides. Surprisingly, even with the collision gas present, the distribution of sizes does not extend to oxide clusters containing more than about five metal atoms. Additionally, the signals observed under these cation growth conditions are relatively small.

Because the cation growth conditions do not produce large densities of clusters and because large metal oxides do not form under these conditions, we have also studied clusters that grow as *neutrals* and are detected by ultraviolet photoionization with an excimer laser. The photoionization behavior of pure metal antimony and bismuth clusters has been investigated extensively by our research group several years ago.[12] At the 193-nm ArF excimer laser wavelength, most of the pure metal species require at least two photons for photoionization. The ionization potentials are believed to be about 7−8 eV,[11,12] and therefore absorption of two photons at 193 nm places about 5 eV of excess energy into the cluster, which often leads to fragmentation. Fragmentation is also more efficient at higher laser powers. When there is extensive fragmentation of a cluster distribution, the masses that remain prominent are the cation species which are most stable and are able to resist fragmentation more effectively. Therefore, our previous work showed that the mass distributions from direct cation growth and those from multiphoton ionization of neutrals were often quite similar. Both experiments lead to preferential formation of species that are stable as cations. An added caveat is that photoionization may also produce abundant mass peaks for clusters that are abundant as neutrals, but that have relatively high ionization cross sections (perhaps from a low ionization potential). Photoionization is therefore not as clean an experiment as direct ion growth in establishing the stable cluster charge states.

Figure 4 shows the metal oxide cluster distributions measured for antimony and bismuth with 193-nm photoionization. The signals observed under these conditions are quite large, suggesting that cluster growth in our nozzle source produces much more neutral clusters than it does cations. The masses detected here do extend out to somewhat larger cluster sizes, but there are still no clusters observed with more than about 9 or 10 metal atoms. The species formed are quite interesting. In addition to the pure metal species, there are prominent oxides detected at the stoichiometries 3/4, 5/7, and 7/10 for both metals. Additional oxides are more or less prominent for one metal, including species such as $Sb_4O_6^+$, $Sb_6O_9^+$, $Sb_9O_{14}^+$, $Bi_5O_{11}^+$, and $Bi_6O_{10}^+$. The 9/14 species detected for antimony under these conditions is also detected under desorption and direct cation conditions, but the other stoichiometries are not observed in the other experiments. Other prominent oxides detected in direct cation growth, such as the 4/5 species, are not noticeable here. However, it is understandable that there would be some differences in the species detected by direct ion growth versus photoionization of neutrals due to the complex dynamics of photoionization, as discussed above. It is therefore likely that at least some of these new stoichiometries may be due to abundant neutrals detected efficiently by photoionization. However, we cannot rule out the possibility of different growth mechanisms for cations and neutrals. We will come back to these species detected only with MPI in the discussion below. It is significant, however, that all three of the different experiments designed to produce cluster cations produce the

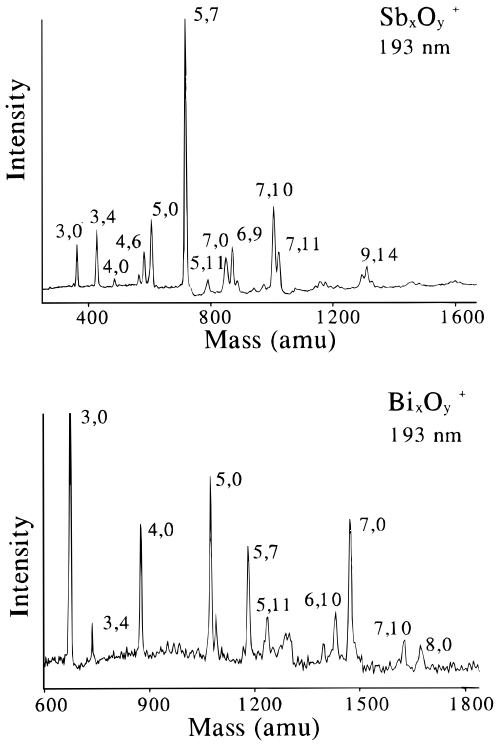

Figure 4. Mass distribution of antimony/oxygen and bismuth/oxygen neutral clusters detected with multiphoton ionization at 193 nm.

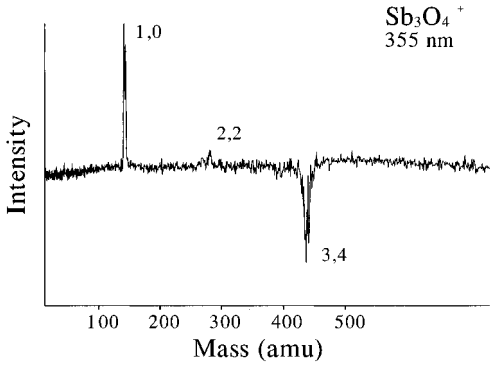

Figure 5. Photodissociation mass spectrum obtained when the cation $Sb_3O_4^+$ is mass-selected and excited at 355 nm. The data are collected with a computer difference technique where the signal is averaged for multiple cycles of PD laser (off−on). The negative peak represents parent ion depletion, and the positive peaks represent the cation photofragments.

3/4, 5/7, 7/10, and 9/14 species preferentially. This is convincing evidence for the thermodynamic stability of these clusters as cations.

An additional technique used to investigate cluster stability in our laboratory is mass-selected photodissociation.[27] This experiment is only available at present in our lab on the molecular beam machines and not on the laser desorption instrument. The molecular beam experiments on direct ion cluster growth (Figure 3) produce signal levels that are two low for mass-selected photodissociation. Therefore, we use the stronger cluster signals produced from the photoionization of neutrals, as in Figure 4. Figure 5 shows the mass-selected photodissociation mass spectrum of Sb_3O_4+ at 355 nm. This figure is the result of a computer difference method for collecting photodissociation spectra, where the intensity of the parent ion signal with no dissociation laser present is subtracted from the parent+fragment ion signals measured when the photodissociation laser is turned on. The resulting spectrum shows a negative peak representing parent ion depletion and a positive peak representing the photofragments. There are therefore only two charged fragments from the $Sb_2O_4^+$, parent ion: a weak peak at $Sb_2O_2^+$ and the atomic Sb^+ ion. The 2/2 cation cluster was also observed in the cation distribution (Figure 3). This fragmentation process and the others indicated below are insensitive over a wide range of fragmentation laser powers. This fragmentation to form mostly the atom is somewhat surprising. It is usually true that larger clusters have lower ionization potentials than atoms, and if an atom is ejected, it would therefore likely be neutral. However, since the neutral fragments are not detected, we do not know if they are molecular or atomic in nature. Additional speculation about this particular fragmentation process is not warranted. However, $Bi_3O_4^+$ produces exactly the same fragmentation pattern, except that there is no weak 2/2 fragment channel.

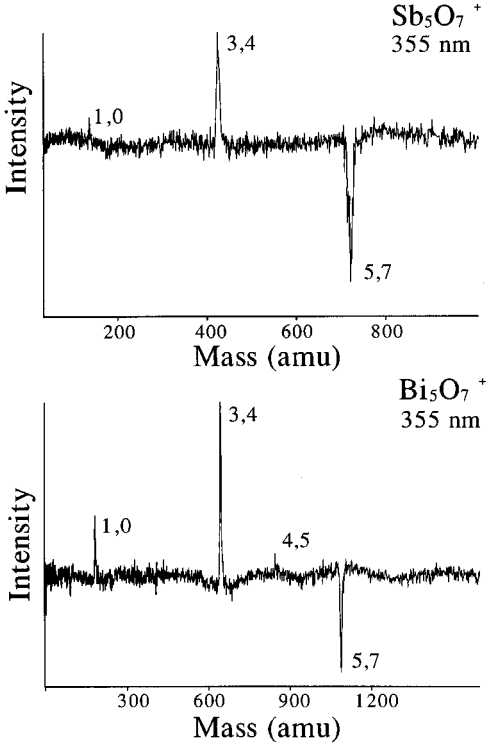

Figure 6. Photodissociation mass spectrum of mass-selected $M_5O_7^+$ clusters for antimony and bismuth. The two isoelectronic metal analogues have essentially the same fragmentation pattern. Both produce the $M_3O_4^+$ fragment.

Figure 6 shows the same kind of photodissociation experiment for the 5/7 parent cations of both metals, also with excitation at 355 nm. As shown, the behavior of the two metal analogues is almost identical, with the $M_3O_4^+$ fragment measured as the most prominent one for both metals. Although we do not detect the neutrals eliminated in this process and cannot distinguish between atomic or molecular neutral fragments, the decrease in mass is M_2O_3, which is exactly the stoichiometry of the bulk oxides for these two metals.

Figure 7 shows the photodissociation for the $M_7O_{10}^+$ clusters, which are the largest oxides we are able to study with photodissociation at present. In these spectra, there are similarities between the two metals, but also noticeable differences. Both species produce the 3/4 cation as a strong fragment ion, but the larger mass fragment from $Sb_7O_{10}^+$ is $Sb_4O_5^+$, while that from $Bi_7O_{10}^+$ is $Bi_5O_7^+$. Smaller fragments include the 2/2 observed for antimony and the 1/0 and 1/1 species observed for bismuth. As discussed above, the 3/4, 4/5, and 5/7 cations are produced preferentially in the growth distributions for both metals. However, there are apparently some energetic or dynamic preferences which cause the decomposition dynamics

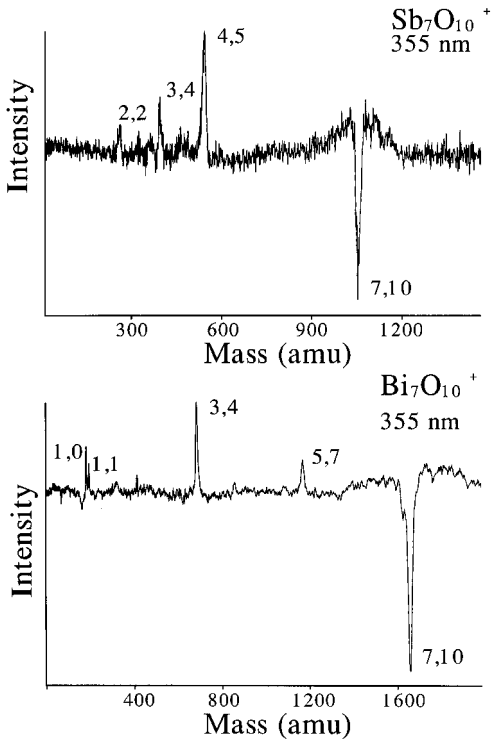

Figure 7. Photodissociation mass spectrum of mass-selected $M_7O_{10}^+$ clusters for antimony and bismuth.

of the larger clusters to be somewhat different. The reason for the preference for the 4/5 oxide fragment for antimony and the 5/7 for bismuth is not clear. It is not possible to determine whether these dissociation processes are sequential or concerted. However, a sequential process would make some sense for the $Bi_7O_{10}^+$ parent. Production of the 5/7 fragment could take place by elimination of Bi_2O_3 as a neutral, and this is the same leaving group postulated above for the production of 3/4 from 5/7. Production of the 4/5 cation fragment from $Sb_7O_{10}^+$ would suggest the elimination of neutral Sb_3O_5 or some combinations of smaller masses adding to this. There is no obvious relationship to the stoichiometry of other ions observed in the source distribution or to the known bulk stoichiometry in this case. However, while the specific channels seen are somewhat curious, it remains true that the prominent cation photofragments measured do indeed correspond to prominent cation clusters formed by cluster growth. Production in these independent experiments confirms that species such as $M_3O_4^+$, $M_4O_5^+$, and $M_5O_7^+$ are indeed cation clusters with special stability. We cannot confirm the preferred stability of the larger clusters (e.g., $M_7O_{10}^+$, $M_7O_{14}^+$) by fragmentation experiments because we cannot generate enough density of these species for the photofragmentation experiments. However, the general agreement between fragmentation experiments and cluster growth experiments suggests that the clusters that appear preferentially in cluster growth are likely to represent especially stable species. Thus, clusters such as $M_7O_{10}^+$, $M_7O_{14}^+$, $M_9O_{14}^+$, $M_9O_{18}^+$, and $M_{11}O_{17}^+$, may be regarded as stable cations because they appear under the direct cation growth conditions and are also seen in some cases in the multiphoton ionization of neutrals.

The species $Sb_4O_6^+$, $Sb_6O_9^+$, $Sb_7O_{11}^+$, $Bi_5O_{11}^+$, and $Bi_6O_{10}^+$ are observed under multiphoton ionization of neutrals, but not as species produced directly in cation growth or by fragmentation of larger mass-selected cations. The origin of these clusters could be neutral species produced with enhanced abundance and not fragmented by the laser, or they could be the result of MPI fragmentation of larger neutral clusters which exhibit dissociation processes not accessible in the other experiments here. We explore these possibilities further below as we develop possible bonding descriptions for these clusters.

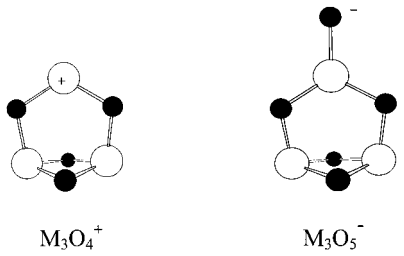

Figure 8. Structures proposed for the $M_3O_4^+$ and $M_3O_5^-$ clusters.

The preferences for certain stoichiometries in these metal oxide clusters are so dramatic that they require some reasonable explanation. Because the patterns are different for the same sized clusters in different charge states and because the isoelectronic metals antimony and bismuth exhibit similar patterns, it is most likely that there is an electronic structure explanation for these tendencies rather than a geometric one. We therefore consider the possibilities for electronic structure effects in these clusters. Electronic structure is the primary consideration for the bonding in the Zintl ion clusters discussed earlier. However, it is immediately evident that the oxide species here do not follow the patterns exhibited by the Zintl ions. The Zintl ion analogues studied before combine group IV and group V elements and are able to overcome their intrinsic electron deficiency by sharing electron density in multicenter bonding. The oxides here combine group V and group VI elements and are not electron deficient. Moreover, there is no similarity to the stoichiometries expected for Zintl ions. We therefore turn to other considerations. Both antimony and bismuth form stable oxide compounds that are routinely available. The stoichiometry in these solid phases is M_2O_3, implying a covalent bonding network with oxidation states of 3+ for the metal and 2− for oxygen. No stable clusters of antimony or bismuth oxides are previously known, but the isoelectronic element phosphorus forms stable clusters which have been isolated and characterized, e.g. P_4O_6.[16] The bonding in these solids or their related clusters are similar. It consists of a network of M−O−M bonding; that is, there are no metal−metal bonds. This is understandable because M−O bonding is much stronger than M−M bonding for the metals antimony and bismuth.[32] If we assume that this same kind of scheme is operative here, we are able to obtain reasonable structures for most of these magic number clusters.

Figure 8 illustrates the structural scheme proposed for the cation and anion clusters containing three metal atoms. The stoichiometries measured for these species are $M_3O_4^+$ and $M_3O_5^-$, respectively. The structure shown for the cation consists of three metal atoms, each with a 3+ valence, and four oxygen atoms, each with a 2− valence. The structure indicated has two metal atoms, which each form three M−O bonds, while the third metal atom, which is in the apex position, forms only two M−O bonds and has a localized excess positive charge. This connectivity satisfies the valence exactly for all the atoms by making two-electron single bonds at all positions. Additionally, it places the atoms in approximately the orientations expected for near-90° angles between adjacent M−O bonds, as would be expected for p-type bonding. The anion follows the same approximate scheme except that there is an additional oxygen. This is bound to the apex atom, giving this metal three M−O bonds, and the terminal oxygen carries the excess negative charge. We are not suggesting that these structures have been measured or indeed that there is any direct evidence for them. However, these connectivity patterns and the qualitative aspects

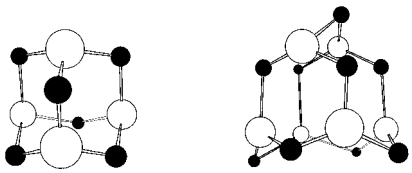

M_4O_6 M_6O_9

Figure 9. Structures proposed for the M_4O_6 and M_6O_9 neutral metal oxide clusters seen here. The 4/6 structure is the same as the already known species P_4O_6, and it has the same general structure as adamantane.

of these structures are the only way to achieve "simple" covalent bonding to rationalize the abundant masses observed for the three-metal atom clusters. The essential features of these structures (M−O−M bonding and bond angles near 90°) that we have proposed have now been confirmed by ab initio calculations by Reddy and Jena.[33] This kind of bonding is attractive because it agrees with the known structural tendencies of the related P_4O_6 cluster and because it explains the sharp preference for a specific stoichiometry corresponding to each specific charge state. The bonding scheme proposed is also unique. No other connectivity is possible for these small clusters which provides a closed shell bonding arrangement for each atom.

This same general kind of bonding can be extended to the larger clusters described here, and reasonable bonding schemes also result for these species. Figure 9 shows the M_4O_6 and M_6O_9 species which are only detected in the experiment by ionization of neutrals. The conditions of their detection suggest that these species might exist as neutrals in the experiment, and if we make this assumption, the bonding makes sense. The M_4O_6 cluster is completely analogous to P_4O_6, which has been isolated and characterized previously. We therefore assume the same structure determined for P_4O_6, which is the adamantane-type cage. As discussed above, this cluster has only M−O−M bonding, with 3+ metal valence and 2− oxygen valence producing a closed shell single-bond network. The 4/6 stoichiometry is also exactly $(M_2O_3)_N$, where $N = 2$, i.e., a multiple of the known bulk phase stoichiometry. M_6O_9 is likewise a multiple of the bulk stoichiometry where $N = 3$ and again a closed shell single-bond network can be assembled with M−O−M bonding. The importance of this 2/3 bulk ratio in the gas phase clusters is also demonstrated in the photodissociation data (Figures 6 and 7), where the M_2O_3 mass is apparently the neutral fragment eliminated. In these examples also, we do not presume to have measured the structures or to have any direct evidence for them. However, while the qualitative structures may not be completely accurate in every detail, it is true that these specific connectivities are unique in providing closed shell bonding networks for these stoichiometries.

Figure 10 shows the structures we propose for even larger cation species indicated by these experiments. The $M_5O_7^+$ and $M_7O_{10}^+$ species both have stoichiometries that indicate that the metal atoms have the same 3+ valence described above. We therefore show structures with each metal atom except one having three M−O bonds. The unique metal atom at an apex site in each structure forms two M−O bonds and carries the excess positive charge. As before, these are only proposed structures and there may be other arrangements (i.e., relative atom positions) that also fulfill the bonding. However, we believe that the connectivities shown here are again unique for these stoichiometries. Unfortunately of course, as cluster size increases, it becomes more difficult to be sure of uniqueness.

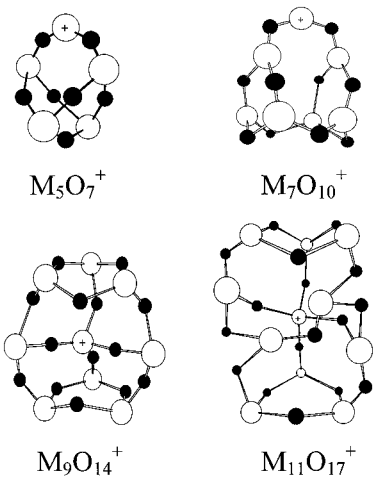

$M_5O_7^+$ $M_7O_{10}^+$ $M_9O_{14}^+$ $M_{11}O_{17}^+$

Figure 10. Structures proposed for several of the larger metal oxide clusters observed here for antimony and bismuth.

The $M_9O_{14}^+$ and $M_{11}O_{17}^+$ clusters are among the largest species for which we have good experimental evidence. Since these clusters are formed preferentially, we presume that a stable bonding arrangement must be possible, as discussed above. However, simple consideration of the stoichiometries immediately suggests that some new bonding scheme must be operative. It is not possible to balance the metal−oxygen charges in these systems unless at least one metal atom has a 5+ charge state. There is tentative evidence in Figure 1 for a cluster at $Bi_{13}O_{20}^+$, and this cluster also must have one 5+ metal. There is also evidence in Figure 1 for clusters at the 7/14, 7/18, 9/18, and 9/22 stoichiometries, and these species must have additional 5+ metal atoms for the clusters to have closed shell configurations. Of these species, the 7/14 cluster appears most intense in Figure 1. This species should have three Bi^{3+} and four Bi^{5+} atoms to achieve a closed shell M−O−M network. For the weaker mass at the stoichiometry 7/18, no combination of Bi^{5+} can balance the stoichiometry unless there is some new bonding scheme (−M−O−O−M−?).

The structures shown in the lower half of Figure 10 illustrate our attempt to rationalize how the bonding might occur in the 9/14 and 11/17 species. These structures are the result of extensive model building, and they are believed to provide unique solutions to the respective single-bonding networks. The clusters are both constructed with the single 5+ metal atom in a central tetrahedral site, forming four M−O bonds and carrying the excess unit of charge. In the 9/14 cluster, there are two six-membered rings situated above and below the central atom, connected by O−M−O bridges on each side. The 11/17 cluster has a more complex structure, which is difficult to visualize without a three-dimensional model. It also consists of a central 5+ metal with rings above and below connected by bridging ring systems. The logical question about these structures concerns their uniqueness, which is difficult to answer definitively. We have searched extensively for other bonding connectivities with which to satisfy valence for all the atoms, but no additional structures are immediately evident. However, we cannot discount the possible existence of other such structures. We certainly do not claim that the specific bonding angles indicated are actually those in the clusters. These are drawn as indicated in the figure to obtain the best symmetry and the best 3-D projection for the figure. The point of these proposed structures is that there are indeed reasonable closed shell bonding arrangements in relatively compact geometric structures that might explain the preferred cluster masses observed.

As indicated here, many of the prominent metal oxides suggested by our experiments have possible structures consisting of M−O−M bonding networks which produce closed shell electronic configurations. This is true for positive ions, negative ions, and neutral clusters. From the consideration of the bonding and the metal valence electron configuration (s^2p^3) some general concepts become apparent. Only clusters with an even number of metal atoms can produce a cluster oxide with a closed shell electronic configuration as a neutral, and only clusters with an odd number of metal atoms can produce a cluster that is closed shell as a cation or anion. Essentially all the prominent clusters observed in this experiment are consistent with this suggestion; that is the species Sb_4O_6 and Sb_6O_9 are proposed as stable neutrals having the general formula $(M_2O_3)_N$, and the species $M_3O_4^+$, $M_3O_5^-$, $M_5O_7^+$, $M_7O_{10}^+$, $M_9O_{14}^+$, and $M_{11}O_{17}^+$ are proposed as stable ions. The relationship between ions and neutrals can be further elucidated if one recognizes that the cation magic number masses 3/4, 5/7, and 7/10 follow the general formula $(M_2O_3)_NMO^+$ for $N = 1, 2, 3$. In other words, the presence of the positive charge dictates that the stoichiometry must be different from the exact bulk value of 2/3, but the increment proceeding to larger sizes is the 2/3 mass. This same 2/3 mass is eliminated as a fragment in the photodissociation experiments. The larger clusters which contain a single M^{5+} atom (9/14, 11/17, 13/20) follow another pattern, with the general formula $(M_2O_3)_NMO_2^+$ for $N = 4, 5, 6$. The increment in cluster growth is again the bulk stoichiometry M_2O_3. The cluster mass $Sb_7O_{11}^+$, which is only observed under photoionization of neutrals (Figure 4) and whose origin was unsure before, can then be included as a member of this series where $N = 3$. The very weak cluster mass $Bi_9O_{18}^+$ seen under cation conditions (Figure 1) and presumed to have five M^{5+} atoms would follow the formula $(M_2O_3)_NMO_6^+$ for $N = 4$.

Two clusters that are apparently anomalous are the $M_4O_5^+$ and $M_6O_8^+$. These 4/5 and 6/8 species are observed for both antimony and bismuth in the direct production of cations (Figure 1), and the 4/5 cluster is produced preferentially for antimony in the fragmentation of larger clusters (Figure 7). All these observations are consistent with the assignment of these two clusters as stable cations. However, since they both contain an even number of metal atoms, both of these cluster cations have an odd number of valence electrons. It is unusual in main group cluster studies to have enhanced stability where a closed shell electron configuration is not possible, but this is apparently the case here. Both of these clusters are small enough to be studied by theory, and they are logical targets that should be investigated.

Two general trends are evident from this line of reasoning. All the clusters here, with the possible exception of the 4/5 and 6/8 species, have as their basic building block the M_2O_3 unit, which is the bulk phase stoichiometry. The specific M_2O_3 cluster for antimony and bismuth is itself an especially stable unit according to theory,[33] having a structure in which two metal atoms are bridged by three oxide bonds. It is therefore reasonable that this would be a good leaving group in fragmentation experiments. However, although the larger clusters add this unit as they grow, it is integrated into the cluster framework so that there is no structural similarity to this molecule in the larger clusters. The second general principle is that the metal valence gradually shifts as one proceeds to larger clusters, i.e., the cluster has an increasing degree of oxidation. All the small clusters have all the metal atoms in the 3+ oxidation state, while this shifts over in the larger clusters to those having one 5+ metal. There is some evidence for larger species having two or more metals in the 5+ state (e.g., $Bi_9O_{18}^+$). Moreover, if our proposed structures have any basis in reality, the higher oxidation state metals reside in the interior of the cluster. This tendency seems to be at odds with trends measured previously for other kinds of clusters. It seems to be generally true that as clusters grow larger, they begin to converge to the properties of the corresponding bulk phase. In these metal oxide species, the smallest clusters already approximate the bulk phase stoichiometry as closely as possible within the limits of their charge. As they grow to larger cluster sizes the stoichiometry shifts *away* from the bulk value. Presumably there is some larger cluster size regime where the stoichiometry of the bulk again becomes favorable.

The experiments here provide the initial evidence for a new class of stable clusters, and we are able to speculate with some success about the electronic structure in these species. If our thinking has any validity, this system of metal oxide clusters may have potential for the isolation of macroscopic materials. The species suggested as stable cations and the species suggested as stable neutrals appear for the most part to be closed shell electronically and they should therefore be relatively inert. The data here primarily address cations, but some information is provided for neutrals. Neutral species of the form $(M_2O_3)_N$ would therefore be likely targets for the preparation of macroscopic materials. Even the ionized species may be viable candidates for isolation if suitable counterions can be found. Theoretical investigations of these species have already begun, and such studies will be extremely important to understand the bonding in these species. However, the nature of the large molecules here (multielectron metal atoms) indicates that such calculations will be extremely challenging for theory. Additional experiments in our lab will focus on specific measurements of the properties of these novel clusters, including their reactivity.

Acknowledgment. This research is supported by the Air Force Office of Scientific Research through contracts No. F49620-94-1-0063 and F49620-97-1-0042 as well as the "ASSERT" Supplement, contract No. F49620-94-1-0267.

References and Notes

(1) Knight, W. D.; Clemenger, K.; de Heer, W. A.; Saunders, W. A.; Chou, M. Y.; Cohen, M. L. *Phys. Rev. Lett.* **1984**, *52*, 2141.

(2) Kroto, H. W.; Heath, J. R.; O'Brien, S. C.; Curl, R. F.; Smalley, R. E. *Nature* **1985**, *318*, 162.

(3) (a) Wheeler, R. G.; LaiHing, K.; Wilson, W. L.; Allen, J. D.; King, R. B.; Duncan, M. A. *J. Am. Chem. Soc.* **1986**, *108*, 8101. (b) Wheeler, R. G.; LaiHing, K.; Wilson, W. L.; Duncan, M. A. *J. Chem. Phys.* **1988**, *88*, 2831.

(4) (a) Guo, B. C.; Kearns, K. P.; Castleman, A. W., Jr. *Science* **1992**, *255*, 1411. (b) Guo, B. C.; Wei, S.; Purnell, J.; Buzza, S.; Castleman, A. W., Jr. *Science* **1992**, *256*, 515. (c) Wei, S.; Guo, B. C.; Purnell, J.; Buzza, S.; Castleman, A. W., Jr. *Science* **1992**, *256*, 818.

(5) Guo, B. C.; Castleman, A. W., Jr. *Advances in Metal and Semiconductor Clusters*; Duncan, M. A., Ed.; JAI Press: Greenwich, CT, 1994; Vol. II.

(6) Pilgrim, J. S.; Duncan, M. A. *J. Am. Chem. Soc.* **1993**, *115*, 6958.

(7) Pilgrim, J. S.; Duncan, M. A. *J. Am. Chem. Soc.* **1993**, *115*, 4395.

(8) Pilgrim, J. S.; Duncan, M. A. *J. Am. Chem. Soc.* **1993**, *115*, 9724.

(9) Pilgrim, J. S.; Duncan, M. A. *Advances in Metal and Semiconductor Clusters*; Duncan, M. A., Ed.; JAI Press: Greenwich, CT, 1995, Vol. III.

(10) (a) Muhlbach, J.; Recknagel, E.; Sattler, K. *Surf. Sci.* **1981**, *106*, 188. (b) Sattler, K.; Muhlbach, J.; Pfau, P.; Recknagel, E. *Phys. Lett.* **1982**, *87A*, 418.

(11) Walstedt, R. E.; Bell, R. F. *Phys. Rev. A* **1986**, *33*, 2830.

(12) (a) Wheeler, R. G.; LaiHing, K.; Wilson, W. L.; Duncan, M. A. *Chem. Phys. Lett.* **1986**, *131*, 8. (b) Geusic, M. E.; Freeman, R. R.; Duncan, M. A. *J. Chem. Phys.* **1988**, *88*, 163. (c) Geusic, M. E.; Freeman, R. R.; Duncan, M. A. *J. Chem. Phys.* **1988**, *89*, 223.

(13) (a) Bach, S. B. H.; McElvany, S. W. *J. Phys. Chem.* **1991**, *95*, 9091. (b) McElvaney, S. W.; Nelson, H. H.; Baronavski, A. P.; Watson, C. H.; Eyler, J. R. *Chem. Phys. Lett.* **1987**, *134*, 214.

(14) Polak, M. L.; Ho, J.; Gerber, G.; Lineberger, W. C. *J. Chem. Phys.* **1991**, *95*, 3053.

(15) (a) Gausa, M.; Kaschner, R.; Lutz, H. O.; Seifert, G.; Meiwes-Broer, K. H. *Chem. Phys. Lett.* **1994**, *230*, 99. (b) Gausa, M.; Kaschner, R.; Lutz, H. O.; Seifert, G.; Meiwes-Broer, K. H. *J. Chem. Phys.* **1996**, *104*, 9719.

(16) King, R. B. *Inorganic Chemistry of Main Group Elements*; VCH Publishers: New York, 1995.

(17) Mandich, M. L.; Reents, W. D. In *Atomic and Molecular Clusters*; Bernstein, E. R., Ed.; Elsevier: Amsterdam, 1990; p 69.

(18) Deng, H. T.; Kerns, K. P.; Castleman, A. W., Jr. *J. Phys. Chem.* **1996**, *100*, 13386.

(19) Schild, D.; Pflaum, R.; Sattler, K.; Recknagel, E. *J. Phys. Chem.* **1987**, *91*, 2649.

(20) Bishop, M. B.; LaiHind, K.; Cheng, P. Y.; Peschke, M.; Duncan, M. A. *J. Phys. Chem.* **1989**, *93*, 1566.

(21) Wade, K. *Adv. Inorg. Chem. Radiochem.* **1976**, *18*, 1.

(22) Chen, Z. Y.; Castleman, A. W. *J. Chem. Phys.* **1993**, *98*, 231.

(23) Deng, H. t.; Kerns, K. P.; Castleman, A. W. *J. Phys. Chem.* **1996**, *100*, 13386.

(24) Rao, A. M.; Eklund, P. C.; Cornett, D. S.; Amster, I. J.; Duncan, M. A. *J. Phys. Chem.* **1993**, *97*, 5036.

(25) Brock, L. R.; Pilgrim, J. S.; Robbins, D. L.; Duncan, M. A. *Rev. Sci. Instrum.* **1996**, *67*, 2989.

(26) LaiHing, K.; Wheeler, R. G.; Wilson, W. L.; Duncan, M. A. *J. Chem. Phys.* **1987**, *87*, 3401.

(27) Cornett, D. S.; Peschke, M.; LaiHing, K.; Cheng, P. Y.; Wiley, K. F.; Duncan, M. A. *Rev. Sci. Instrum.* **1992**, *63*, 2177.

(28) (a) Ban, V. S.; Knox, B. E. *J. Chem. Phys.* **1970**, *52*, 243. (b) Ban, V. S.; Knox, B. E. *J. Chem. Phys.* **1970**, *52*, 248.

(29) Shepard, A.; Hewitt, R. W.; Slusser, G. J.; Baitinger, W. E.; Cooks, R. G.; Winograd, N.; Delglass, W. N.; Varon, A.; Devant, G. *Chem. Phys. Lett.* **1976**, *44*, 371.

(30) Sidorov, L. N.; Minayeva, I. I.; Zasorin, E. Z.; Sorokin, I. D.; Borshchevshiy, A. Y. *High Temp. Sci.* **1980**, *12*, 175.

(31) Marschman, S. C.; Lynch, D. C. *Can. J. Chem. Eng.* **1984**, *62*, 875.

(32) Huber, K. P.; Herzberg, G. *Molecular Spectra and Molecular Structure Vol. IV. Constants of Diatomic Molecules*; Van Nostrand Reinhold: New York, 1979.

(33) Reddy, B. V.; Jena, P. Private communication.